Cu isotopes in marine black shales record the Great Oxidation Event

Ernest Chi Fru[a,1], Nathalie P. Rodríguez[a], Camille A. Partin[b], Stefan V. Lalonde[c], Per Andersson[d], Dominik J. Weiss[e], Abderrazak El Albani[f], Ilia Rodushkin[g], and Kurt O. Konhauser[h]

[a]Department of Geological Sciences and Bolin Centre for Climate Research, Stockholm University, SE-10691 Stockholm, Sweden; [b]Department of Geological Sciences, University of Saskatchewan, Saskatoon, SK, Canada S7N 5E2; [c]CNRS-UMR 6538 Laboratoire Domaines Océaniques, Institut Universitaire Européen de la Mer, Université de Bretagne Occidentale, Technopôle Brest-Iroise, Place Nicolas Copernic, Plouzané 29280, France; [d]Department of Geosciences, Swedish Museum of Natural History, SE-104 05 Stockholm, Sweden; [e]Department of Earth Science and Engineering, Royal School of Mines, Imperial College, London SW7 2BP, United Kingdom; [f]Institut de Chimie des Milieux et Matériaux de Poitiers, Université de Poitiers UMR 7285-CNRS, 86073 Poitiers, France; [g]ALS Scandinavia AB, ALS Laboratory Group, S-977 75 Lulea, Sweden; and [h]Department of Earth and Atmospheric Sciences, University of Alberta, Edmonton, AB, Canada T6G 2EG

Edited by Mark H. Thiemens, University of California, San Diego, La Jolla, CA, and approved March 10, 2016 (received for review December 17, 2015)

The oxygenation of the atmosphere ∼2.45–2.32 billion years ago (Ga) is one of the most significant geological events to have affected Earth's redox history. Our understanding of the timing and processes surrounding this key transition is largely dependent on the development of redox-sensitive proxies, many of which remain unexplored. Here we report a shift from negative to positive copper isotopic compositions ($\delta^{65}Cu_{ERM\text{-}AE633}$) in organic carbon-rich shales spanning the period 2.66–2.08 Ga. We suggest that, before 2.3 Ga, a muted oxidative supply of weathering-derived copper enriched in ^{65}Cu, along with the preferential removal of ^{65}Cu by iron oxides, left seawater and marine biomass depleted in ^{65}Cu but enriched in ^{63}Cu. As banded iron formation deposition waned and continentally sourced Cu became more important, biomass sampled a dissolved Cu reservoir that was progressively less fractionated relative to the continental pool. This evolution toward heavy $\delta^{65}Cu$ values coincides with a shift to negative sedimentary $\delta^{56}Fe$ values and increased marine sulfate after the Great Oxidation Event (GOE), and is traceable through Phanerozoic shales to modern marine settings, where marine dissolved and sedimentary $\delta^{65}Cu$ values are universally positive. Our finding of an important shift in sedimentary Cu isotope compositions across the GOE provides new insights into the Precambrian marine cycling of this critical micronutrient, and demonstrates the proxy potential for sedimentary Cu isotope compositions in the study of biogeochemical cycles and oceanic redox balance in the past.

paleoceanography | trace metals | copper cycling | Precambrian | Proterozoic

Shortly after the Archean–Paleoproterozoic boundary, the Great Oxidation Event (GOE) ∼2.45–2.32 billion years ago (Ga) marks the first permanent accumulation of oxygen in Earth's atmosphere (1–4). Evidence for the GOE comes from a convergence of proxies, including the evolution of redox-sensitive element concentrations and their isotopic compositions in marine sedimentary rocks. Accompanying the GOE was an increase in the oxidative weathering of a relatively untapped continental sulfide reservoir and the onset of sulfide-rich (euxinic) water column conditions in marginal marine settings caused by bacterial sulfate reduction of an increasing oceanic sulfate pool (1–8). These events are reflected in the transition from Neoarchean oceans characterized by abundant iron oxide precipitation and the deposition of banded iron formations (BIF) to relative BIF scarcity and increased global marine pyrite burial for much of the Paleoproterozoic (4–13).

Light iron (Fe) isotope enrichments in sedimentary pyrite older than 2.4 Ga records oceans strongly affected by BIF deposition and dissimilatory Fe(III) reduction, whereas generally near-zero to positive Fe isotope compositions between 2.3 Ga and 1.8 Ga reflect near-complete drawdown of the Fe reservoir by enhanced oxidation and/or marine pyrite burial (8, 13). The lack of substantial $\delta^{56}Fe$ variations in black shale pyrite after 1.5 Ga coincides with oceans becoming even less Fe-rich due to waning submarine hydrothermal activity (8–13). To provide a new and complementary perspective on water column redox evolution surrounding the GOE, we turned to sedimentary copper (Cu) isotope compositions, known to respond to redox shifts tuned to Fe and sulfur (S) cycling. Preferential sequestration of ^{65}Cu by iron oxides (e.g., refs. 14–16) precipitated from ferruginous Archean oceans may have enriched seawater in residual ^{63}Cu. We can thus hypothesize that, before the GOE, massive Archean iron oxide precipitation in the form of BIF preferentially buried ^{65}Cu, enriching residual seawater in ^{63}Cu. Conversely, oxidative continental weathering of sulfides, such as chalcocite (Cu_2S) and chalcopyrite ($CuFeS_2$), should have increased the supply of dissolved Cu(II) and delivered more ^{65}Cu-rich runoff to the oceans (17–27) after the GOE. Oxidative dissolution of Cu(I) sulfide minerals to dissolved Cu(II) entails Cu isotope fractionation between the reservoirs by up to 1.2–3.1‰ [$\Delta^{65}Cu_{(Cu(II)\text{–}Cu(I)\ sulfide)}$] (26). Moreover, Cu isotope fractionations between surface/groundwater, secondary Cu minerals, and primary Cu sulfide sources all enrich the aqueous phase in ^{65}Cu, yielding fractionations up to 12‰ between dissolved Cu and its source (26). Riverine supply of waters enriched in ^{65}Cu as the result of continental sulfide oxidation (1–12) should have influenced the highly productive post-GOE marginal

Significance

Redox-sensitive transition metals and their isotopes provide some of the best lines of evidence for reconstructing early Earth's oxygenation history, including permanent atmospheric oxygenation following the Great Oxidation Event (GOE), ∼2.45–2.32 Ga. We show a shift from dominantly negative to permanently positive copper isotope compositions in black shales spanning ∼2.66–2.08 Ga. We interpret the transition in marine $\delta^{65}Cu$ values as reflecting some combination of waning banded iron formation deposition (which removes heavy Cu) and increased oxidative delivery of Cu from continental sulfides (which supplies heavy Cu). Both processes are ultimately related to increased oxidative weathering and a progressive increase in sulfate and sulfide availability accompanying the GOE. Our results provide insights into copper cycling and bioavailability coupled to Earth's oxygenation history.

Author contributions: E.C.F. designed research; E.C.F., N.P.R., C.A.P., and S.V.L. performed research; E.C.F., C.A.P., S.V.L., P.A., A.E.A., I.R., and K.O.K. contributed new reagents/analytic tools; E.C.F., N.P.R., C.A.P., S.V.L., P.A., D.J.W., and K.O.K. analyzed data; and E.C.F., N.P.R., C.A.P., S.V.L., D.J.W., and K.O.K. wrote the paper.

The authors declare no conflict of interest.

This article is a PNAS Direct Submission.

[1]To whom correspondence should be addressed. Email: ernest.chifru@geo.su.se.

This article contains supporting information online at www.pnas.org/lookup/suppl/doi:10.1073/pnas.1523544113/-/DCSupplemental.

marine basins. We can thus hypothesize that the GOE should be accompanied by a transition to seawater that is enriched in ^{65}Cu relative to continental sources, similar to the modern ocean (28). This ^{63}Cu, in turn, would have become incorporated into planktonic biomass that scavenged Cu from seawater. After the GOE, increased oxidative weathering of a previously unweathered continental sulfide pool (5) should have progressively delivered isotopically heavy riverine Cu(II) to the oceans as iron oxide deposition waned in the face of increasingly common oxic or euxinic conditions.

Collectively, this sequence of events predicts that sedimentary $\delta^{65}Cu$ values should have become increasingly positive across the GOE. To test this hypothesis, we selected a suite of well-characterized, low metamorphic grade black shale samples deposited before, during, and after the GOE, spanning ~2.7–2.1 Ga. The samples span the Transvaal Supergroup in South Africa and the Francevillian Series in Gabon, both of which have been widely used for reconstructing key intervals in Earth's oxygenation (1, 7, 29–31). Our coeval $\delta^{56}Fe$ (redox-sensitive proxy), $\delta^{13}C_{org}$ (biological activity proxy), and $\delta^{65}Cu$ records, spanning Late Archean iron-rich to Paleoproterozoic sulfide-rich marginal ocean conditions, provide new insight into the Precambrian cycling of Cu, a critical micronutrient, as well as the proxy potential of $\delta^{65}Cu$ for tracing marine paleoredox.

Results and Discussion

Temporal Changes in Sedimentary Cu Dynamics on the Evolving Earth. Changes in the sources, sinks, and mechanisms of Cu delivery to Archean and Paleoproterozoic oceans would have affected both biological activity and Cu isotopic composition. To interpret the $\delta^{65}Cu$ data, we first reconstruct temporal Cu sedimentary concentrations and the relative importance of iron and sulfide sinks from the BIF and black shale archives (Fig. 1). The shale and BIF records of authigenic Cu enrichment (Fig. 1 *A* and *B*), normalized to detrital input using Ti (e.g., refs. 5, 22, and 32), are remarkably static, showing insignificant change on either side of the GOE. Authigenic Cu enrichment in BIF is ~1,000 times higher relative to black shale (Fig. 1*C*). After the GOE, BIF deposition decreased by approximately three orders of magnitude in terms of tonnage (Fig. 1*D*), likely associated with declining hydrothermal activity and increasing marine sulfate content resulting from enhanced oxidative continental sulfide weathering (1–13). Consequently, during peak BIF deposition, BIF likely exerted a stronger influence on the concentration and isotope composition of dissolved Cu than black shale deposits. Moreover, Cu/Ti molar ratios in black shale generally fall within an order of magnitude of the upper continental crust (Fig. 1*C*), implying that black shales are not a strong Cu sink and therefore are not expected to influence the Cu isotope budget to the same degree as iron oxide-rich sediments.

Temporal Changes in Sedimentary Cu Isotopic Compositions. Predominantly negative $\delta^{65}Cu$ values in ferruginous late Archean oceans increase from –0.55‰ to +0.74‰ by ~2.3 Ga, after which $\delta^{65}Cu$ values ≤ 0‰ disappear from our shale record (Fig. 2*A*, Table 1, and Fig. S1). This irreversible upward stratigraphic change, which points to secular modification of seawater chemistry from the Neoarchean to the Paleoproterozoic, is significant at the 95% confidence interval (ANOVA, $P < 0.05$). The $\delta^{65}Cu$ values appear to plot inversely to $\delta^{13}C_{org}$ with respect to time (Fig. 2*B*), suggesting covariance in Cu and C cycling in ancient oceans.

The preferential adsorption of dissolved ^{65}Cu by iron oxides yields a $\Delta^{65}Cu_{solution\text{-}iron\ oxide}$ fractionation of up to ~1‰ (14–16). During peak BIF deposition at ~2.48 Ga, ~4.5×10^{12} mol Fe/y may have been removed by iron oxide sinks, thereby also removing ~1×10^8 moles of Cu from the ocean annually (33). Residual bioavailable Cu in the water column would have been left enriched in the lighter isotope ^{63}Cu. This appears reflected in the Neoarchean data, where black shales reach the lowest $\delta^{65}Cu$ values in our dataset. With the dramatic reduction in BIF deposition by a factor of 1,000 across the GOE (Fig. 1*D*), a shift to heavy dissolved marine ^{65}Cu enrichment appears inevitable. Shale $\delta^{65}Cu$ values (tracking seawater) may readily be explained by Rayleigh distillation across important shifts in the proportion of marine Cu exiting via iron oxide sinks (Fig. 3). Similar isotopic distillation of Cu occurs today in supergene weathering environments (14). Indeed, starting from seawater with a modern Cu isotopic composition of ~0.5‰, $\delta^{65}Cu$ values as low as those observed between 2.5 Ga and 2.45 Ga cannot be achieved during

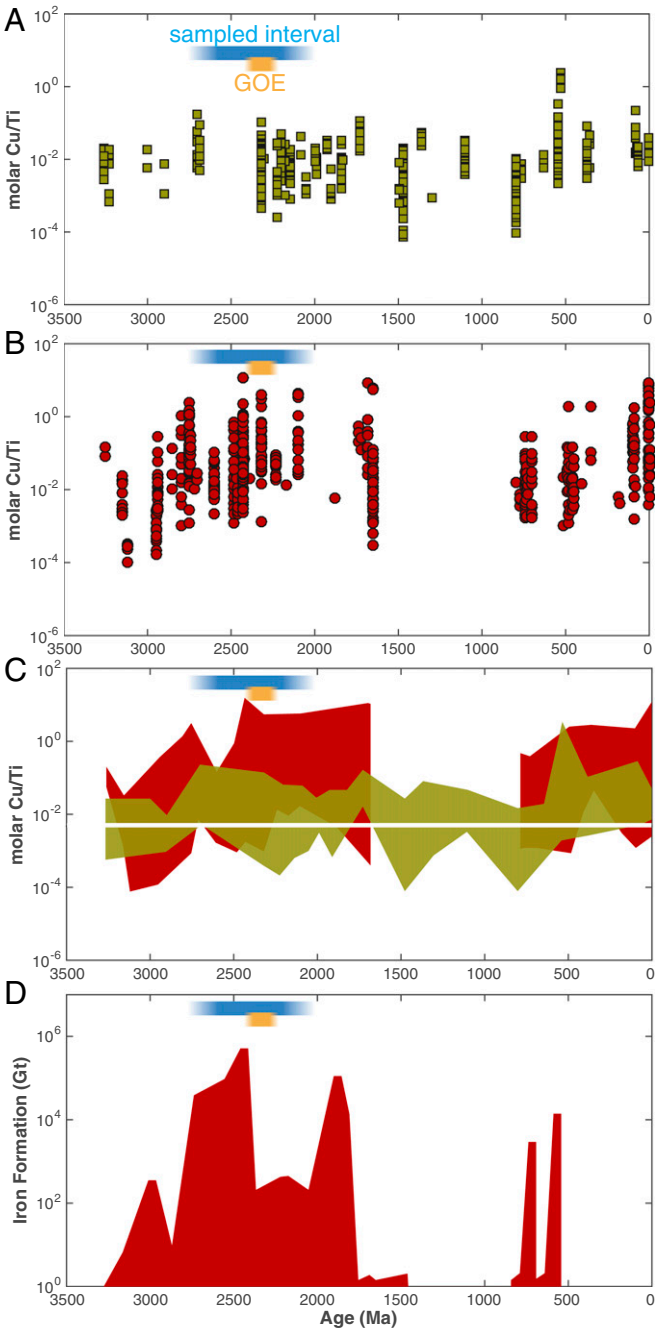

Fig. 1. Copper distribution in banded iron formations and black shales throughout Earth history (see *Supporting Information* and Datasets S1 and S2 for details). (*A* and *B*) molar Cu/Ti ratios in shales (*A*) and banded iron formations (*B*). (*C*) Their enrichments compared (black shale in green, BIF in red), relative to the average continental crust (white line). (*D*) BIF tonnage over time, data from ref. 11.

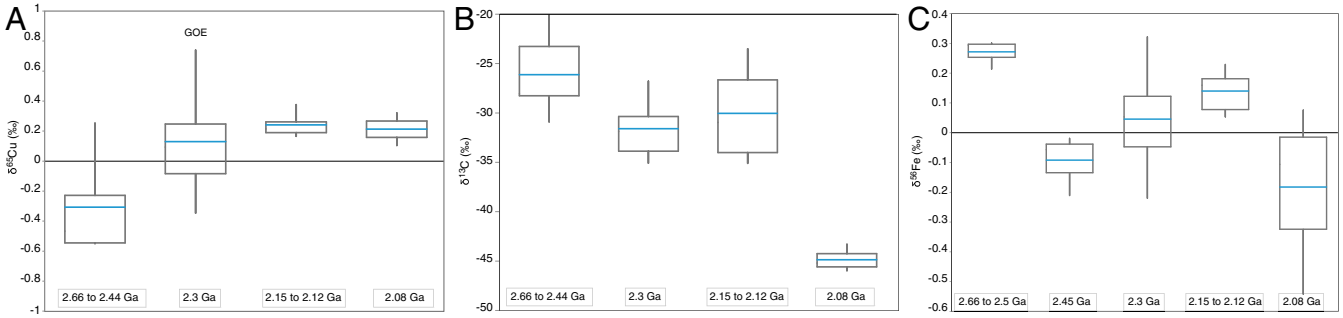

Fig. 2. Box and whisker isotopic plots ($\delta^{65}C$, $\delta^{13}C_{org}$, $\delta^{56}Fe$) across the GOE interval. (*A*) The $\delta^{65}Cu$ values in ~2.7–2.0 Ga black shales, showing a transition to heavier values with the onset of the GOE. (*B* and *C*) Corresponding $\delta^{13}C_{org}$ (*B*) and $\delta^{56}Fe$ (*C*) values. See *Supporting Information* for details of analysis.

adsorption to iron oxides in the absence of open-system behavior (Fig. 3).

Moving into the GOE, increasing sedimentary $\delta^{65}Cu$ relative to the Neoarchean may also be partially explained by an increasing supply of isotopically heavy Cu via continental sulfide weathering (17–27) due to atmospheric oxygenation. Abiotic and biotic oxidation of Cu minerals by O_2 produces a solution enriched in ^{65}Cu, with a $\Delta^{65}Cu_{solution\text{-}source\ mineral}$ value up to ~3‰ (14, 17–27). Cu isotope fractionation during precipitation of secondary Cu minerals further enriches the aqueous phase in ^{65}Cu, leading to a cumulative fractionation of up to 12‰ between dissolved Cu and its source (26).

Although shifts in both source Cu isotopic composition and the importance of iron oxide sinks may have influenced the sedimentary $\delta^{65}Cu$ record, the Cu enrichment records in both shales and BIF are relatively static (Fig. 1 *A* and *B*), which indicates a more important role for the latter. Our data imply that the light Neoarchean $\delta^{65}Cu$ values are best explained by inheritance from a seawater component that was isotopically enriched in ^{63}Cu due to ~200 million years of intense BIF deposition that preferentially removed ^{65}Cu (Fig. 4*A*). After the GOE, the reduction in BIF deposition, coupled to increased acid rock drainage on land related to the oxidation of sulfide minerals (5), changed the Cu isotopic composition of seawater to permanently positive values.

The adsorption and uptake of dissolved Cu by bacteria appears to favor the light isotope at acidic pH. However, a negligible isotopic effect (i.e., $\Delta^{65}Cu_{solution\text{-}phytoplankton} \approx 0$) is consistently observed in the pH range of modern oceans, for both prokaryotes and eukaryotes (16, 28). In our sample suite, $\delta^{13}C_{org}$ values become increasingly depleted with time (Fig. 2*B*), in agreement with reports for other marine sedimentary rocks during this period (3, 34). Anomalously light black shale $\delta^{13}C_{org}$ values at 2.08 Ga have been previously linked to massive oxidation of organic matter and methanotrophy, possibly by the anaerobic oxidation of methane (7, 34–36). The absence of a corresponding shift in the $\delta^{65}Cu$ signal suggests that the biological processes generating anomalously light sedimentary $\delta^{13}C_{org}$ signals are largely decoupled from drivers of the $\delta^{65}Cu$ signal.

Paired Cu and Fe Isotope Records of Marine Redox Evolution. Independent $\delta^{56}Fe$ data from black shale sulfides spanning the

Table 1. Summary of isotopic data

Site	Formation	Depth, m	Age, Ga	Cu_{bulk}, ppm	$\delta^{65}Cu_{bulk}$, ‰	$\delta^{65}Cu_{bulk}$, 2σ	Fe_{bulk}, ppm	$\delta^{56}Fe_{bulk}$, ‰	$\delta^{56}Fe_{bulk}$, 2σ	C_{org}, wt.%	$\delta^{13}C_{org}$, ‰	S_{bulk}, wt.%	$\delta^{34}S_{bulk}$, ‰	$\delta^{15}N_{bulk}$, ‰
Francevillian Basin	FD	10	2.08	413	0.213	0.154	98,733.3	−0.546	0.064	10.9	−45.98	ND	ND	ND
		28	2.08	111.4	0.322	0.178	192,600	−0.11	0.052	8.6	−45.2	4.17	23.99	ND
		70	2.08	92	0.104	0.130	93,600	0.072	0.034	3.1	−43.3	0.9	−0.21	ND
	FB2	228	2.12	126.7	0.165	0.176	39,900	0.225	0.076	5	−35.11	1.03	11.07	4.49
		242	2.12	835.4	0.190	0.122	59,020	0.142	0.066	13.75	−34.16	1.45	14.65	5.74
		282	2.12	394.3	0.262	0.154	42,946.7	0.169	0.044	8.1	−33.58	2.66	11.26	7.48
	FB1	474	2.15	238.1	0.377	0.188	97,800	0.051	0.046	10.9	−26.08	4.03	0.64	ND
		492	2.15	108.3	0.215	0.194	79,400	0.049	0.042	5.59	−23.49	0.34	−23.47	3.26
		697	2.15	138.7	ND	ND	85,466.7	0.18	0.042	0.27	−28.33	0.01	−3.08	−0.3
South Africa	Timeball Hill	85	2.3	88.7	0.225	0.058	17,293.3	0.184	0.042	1.9	−31.01	ND	ND	ND
		180	2.3	845.3	0.741	0.202	138,533.3	−0.054	0.062	1.41	−29.7	0.03	ND	ND
		214	2.3	1954	0.271	0.138	196,466.7	−0.049	0.062	0.95	−26.77	ND	ND	ND
		320	2.3	665.2	−0.347	0.174	1,817,333	0.053	0.048	0.44	−34.79	0.02	ND	ND
		490	2.3	109.7	−0.034	0.102	95,733.3	0.049	0.024	0.49	−35.09	ND	ND	ND
		568	2.3	353.2	−0.134	0.060	100,200	−0.224	0.16	0.75	−31.88	3.7	−25.14	ND
		570	2.3	202.7	0.094	0.120	85,600	0.318	0.08	2.55	−32.93	0.04	−18.46	ND
	Eccles	594	2.44	85.5	ND	ND	191,000	−0.061	0.032	3.43	−23.26	0.02	ND	ND
		1068	2.44	196.3	−0.389	0.276	34,093.3	−0.023	0.044	16.39	−28.06	0.08	0.29	ND
	Lyttleton	1434	2.45	122.7	ND	ND	94,933.3	−0.215	0.108	5.37	−20.1	0.21	−4.42	ND
	Monte Christo	1852	2.50	137.7	−0.543	0.288	82,600	0.289	0.024	8.54	−30.9	0.03	−6.84	ND
		2048	2.50	117.4	0.253	0.106	32,353.3	0.297	0.058	0.3	ND	0.33	−4.78	ND
	Bothaville	2440	2.66	1,344	−0.550	0.174	322,266.7	0.21	0.048	0.88	−28.25	ND	ND	ND

The FD formation was deposited under sulfidic conditions, whereas the FB2 and FB1 are associated with ferruginous conditions (7). The Neoarchean to early Paleoproterozoic sediments would have been formed under more dominant ferruginous conditions (9, 11), whereas the ~2.3 GOE Time Ball Hill shales are linked to sedimentary pyrite deposition (1). ND, not detected; 2σ, 2 SD.

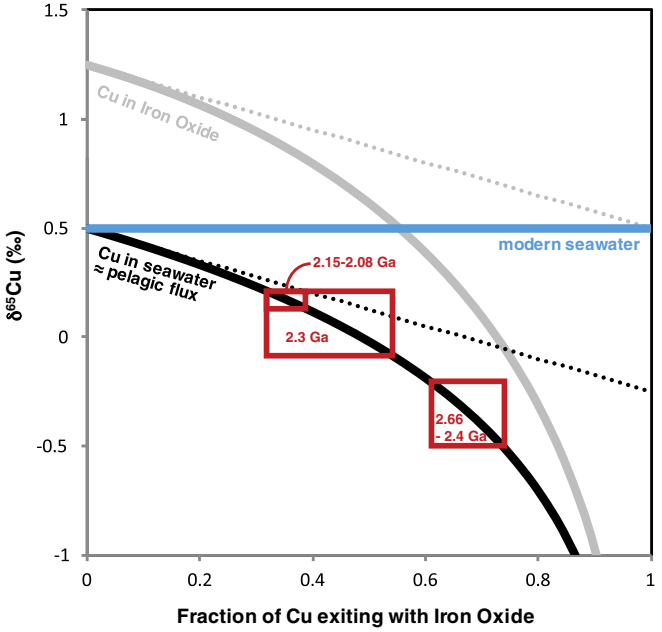

Fig. 3. Rayleigh isotope distillation of δ^{65}Cu between seawater and iron oxide sinks. Black shale δ^{65}Cu values are assumed to reflect contemporaneous seawater composition (28). An experimentally determined Δ^{65}Cu value of 0.75‰ between seawater and iron oxides (14–16) was used to calculate the isotopic composition of Cu sequestered into iron oxides and residual isotopic composition of seawater, assuming an initial δ^{65}Cu of seawater of 0.5‰ in the absence of BIF deposition, similar to modern (28).

GOE show a transition to heavier values (8), similar to our δ^{65}Cu data. This evolution to more positive δ^{56}Fe values in pyrite was suggested to reflect marginalized and near-quantitative precipitation of iron oxides in surface waters, leaving deep ocean waters near δ^{56}Fe = 0 to form isotopically heavier pyrite. Such a scenario is compatible with our δ^{65}Cu data, which also suggest marginalized iron oxide precipitation by 2.3 Ga. Bulk shale δ^{56}Fe values from our own sample set also capture the GOE transition (Fig. 2), but, unlike the pyrite data from ref. 8, they display a complex trajectory from positive to near-zero values between 2.66 Ga and 2.45 Ga, gradually increasing from 2.45 Ga to 2.15 Ga, and returning to more negative and variable values at 2.08 Ga. This complexity is in part due to the local nature of Fe-based proxies (e.g., ref. 37) but also to the fact that, at the bulk rock scale, different environmental processes can generate similar sedimentary Fe isotope compositions. For example, both oxic and sulfidic conditions may cause near-quantitative Fe removal and draw sedimentary Fe isotope compositions toward source values (8, 11, 31, 37), whereas smaller degrees of Fe removal by iron oxide or sulfide precipitation can yield positive sedimentary iron isotope enrichments (8, 38).

For our bulk shale δ^{56}Fe record (Fig. 2), and in light of previous findings regarding the redox history of our sample suite (1, 7, 29–31), we suggest that positive values preserved under ferruginous conditions *ca*. 2.66 Ga likely reflect precipitation of a small portion of the dissolved Fe pool under weakly oxidizing conditions (8); near-zero and variable values *ca*. 2.45–2.15 Ga represent a more important proportion of the local dissolved Fe pool being deposited as iron oxides or sulfides with increasing environmental oxygenation (8); and a return to negative values under euxinic basinal conditions *ca*. 2.08 Ga (7) is best explained by enrichment of light isotopes into iron sulfides formed in the water column or during early diagenesis (38). Across the GOE, differences between our bulk shale δ^{56}Fe values and those reported for pyrites across the same interval (8), as well as the similar evolution of δ^{65}Cu and pyrite δ^{56}Fe but not bulk shale δ^{56}Fe, suggest that δ^{65}Cu and δ^{56}Fe in pyrite are more effective archives of evolving Cu and Fe cycling than is bulk shale δ^{56}Fe.

Implications for Cu Cycling at the Archean–Proterozoic Boundary. The disappearance of δ^{65}Cu values ≤0‰ in shales after 2.3 Ga suggests that Cu isotopes captured a unidirectional shift in the oxygenation of the atmosphere–ocean system across the GOE. Increased riverine Cu and sulfate supply as the result of sulfide mineral weathering across the GOE was accompanied by a decrease in iron oxide precipitation, as evident from the dramatic reduction in BIF (Fig. 1*D*) and increased precipitation of sulfide minerals (1–11) after the GOE. Indeed, our data indicate a coincidental increase in bulk δ^{34}S values and sedimentary S concentrations around ∼2.2 Ga (Table 1 and Fig. S2), consistent with previous studies indicating an expansion of the marine sulfate reservoir after the GOE (1–6). In the face of a waning iron oxide exit channel for isotopically light Cu, the isotopically heavy δ^{65}Cu values in post-GOE shales are readily explained by continental weathering processes (17–27) delivering dissolved riverine Cu with a δ^{65}Cu signature of up to ∼0.7‰ (26, 39–41) to the oceans, as today (28).

The idea that the observed positive shift in δ^{65}Cu values across the GOE may be attributed to both a waning BIF sink and increased delivery of heavy Cu by oxidative weathering may be complicated by episodes in the Neoarchean record ∼2.66–2.45 Ga when sedimentary Cu enrichments in the BIF and shale records may have approached parity, as suggested by coeval Cu/Ti signals (Fig. 1*C*). It is possible that the light δ^{65}Cu values produced during these episodes may reflect the formation of sedimentary Cu sulfides that incorporated isotopically light Cu (17), negating the need for any reduction in the iron oxide sink across the GOE to explain the evolution of the sedimentary δ^{65}Cu signal. However, such a mechanism for the evolution of the δ^{65}Cu signal would require that sedimentary sulfide enrichments were stronger *ca*. 2.66–2.45 Ga and decreased by 2.15 Ga. Our dataset indicates the opposite, with low sedimentary sulfide concentrations *ca*. 2.66–2.45 Ga, increasing significantly as δ^{65}Cu values become permanently positive by 2.15 Ga (Fig. S3), consistent with independent evidence for an increasing marine sulfate reservoir (1–12). We can thus rule out the possibility that the formation of sedimentary Cu sulfides was responsible for isotopically light sedimentary δ^{65}Cu values before 2.5 Ga. The establishment of an oxidative manganese (Mn) cycle ∼2.4–2.2 Ga (42) may further explain why, after the GOE, sedimentary marine δ^{65}Cu values became permanently positive, because Mn(IV) oxides, such as birnessite, preferentially remove ^{63}Cu (39–41). This correlates well with our sample set showing an increase in sedimentary Mn concentrations across the GOE (Fig. S4).

Similar and mostly positive δ^{65}Cu value (up to 0.49‰) characterize Cambrian marine shales formed under euxinic marine conditions characterized by intense bacterial sulfate reduction in a lagoonal transgressive environment (43, 44). These sulfidic depositional conditions are similar to the situation under which the Francevillian FD and Timeball Hill formations were deposited (1, 7). The fact that both show isotopically heavy δ^{65}Cu values indicates that sedimentary sulfides that preferentially incorporate isotopically light Cu (17) either play little role in determining sedimentary δ^{65}Cu composition or, perhaps more likely, that sedimentary sulfides formed during diagenesis quantitatively trap locally available sedimentary Cu without fractionation. In either case, our data indicate that sedimentary Cu isotope systematics may be relatively insensitive to local euxinia. Although the generation of secondary minerals enriched in ^{63}Cu through fluid migration in reworked clastic sediments has been noted (45), such metasomatic processes are not known to have affected our samples (1, 7, 29–31) and cannot explain the secular increase in sedimentary δ^{65}Cu values from ∼2.66–2.3 Ga or the reproducibility of positive sedimentary δ^{65}Cu values after 2.3 Ga. We conclude that some combination of increased oxidative weathering (supplying isotopically heavy Cu) and waning BIF deposition (diminished sink

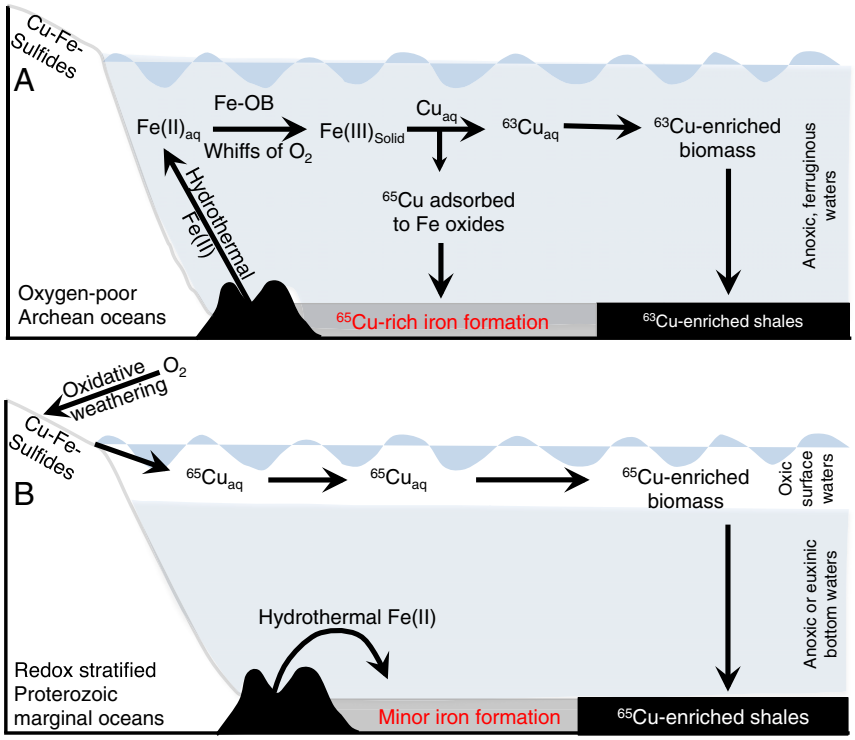

Fig. 4. Conceptual model for Late Archean and Early Proterozoic marine cycling and isotope composition of Cu. (*A*) During the Neoarchean, the marine Cu cycle lacked oxidative weathering inputs and was strongly influenced by iron oxide deposition. (*B*) During the Early Proterozoic, isotopically heavy Cu was supplied by continental weathering of sulfides, while iron oxide sinks waned, both promoting ^{63}Cu depletion from seawater and pelagic sediments. Fe-OB, iron-oxidizing bacteria.

for heavy Cu) is the most likely explanation for the evolution of the sedimentary δ^{65}Cu signal to heavier values across the GOE. The relative roles of these two processes in controlling sedimentary δ^{65}Cu values needs to be further examined in the rock record, and our model provides clear hypotheses for such examination. If the sequestration of isotopically heavy Cu by iron oxides has been more important historically than changes in the oxidative weathering supply of continental Cu, then one would expect a return to lighter values during later events of increased iron oxide deposition, for example during enhanced worldwide rifting and deposition of BIF *ca*. 1.88 Ga (46), or when BIF deposition resumed during the Neoproterozoic Snowball Earth events (11). Alternatively, if a shift in Cu sources controlled the evolving sedimentary δ^{65}Cu signal, then the onset of important oxidative weathering and riverine supply of isotopically heavy Cu across the GOE, and the accompanying transition toward heavier sedimentary δ^{65}Cu values, would represent a unique, secular shift in the marine Cu cycle never to be repeated.

Conclusions

Across the GOE boundary, we observe a consistent trend from negative δ^{65}Cu and positive δ^{56}Fe values during ferruginous conditions toward heavy δ^{65}Cu and light δ^{56}Fe signatures in post-GOE sedimentary successions with greater sedimentary sulfide contents. We interpret the transition in marine δ^{65}Cu values, from negative to positive across the GOE, to reflect some combination of waning BIF deposition (which removes heavy Cu) and increased oxidative delivery of Cu from continental sulfides (which supplies heavy Cu). Both processes are ultimately related to increased oxidative continental weathering and a progressive increase in sulfate and sulfide availability accompanying the GOE. Our dataset reveals a disappearance of negative δ^{65}Cu values from the black shale record after ∼2.3 Ga, when the GOE was at its height, and supports a change from low marine sulfate conditions during the Archean to sulfate-rich oceans after the GOE. The gradual change in our δ^{65}Cu values continues for ∼150 million years after the disappearance of mass-independent sulfur isotope fractionation by ∼2.32 Ga, a key marker of the GOE (1–3, 47), reaffirming that the GOE was a protracted event that took place between 2.45 Ga and 2.3 Ga (1, 8). Finally, this study provides insights into the Precambrian marine cycling of this critical micronutrient and opens avenues for exploring marine paleoredox at different periods during Earth history using stable Cu isotope tracers.

ACKNOWLEDGMENTS. We thank François Gauthier Lafaye for logistical support. This work was funded by a European Union Marie Curie fellowship (Grant PIEF.GA-2010-276475) and partly by the European Research Council (Grant 336092) and the Bolin Centre for Climate Change. K.O.K. thanks the Natural Sciences and Engineering Research Council of Canada for financial support. S.V.L. acknowledges financial support from LabexMER and the Region of Brittany.

1. Bekker A, et al. (2004) Dating the rise of atmospheric oxygen. *Nature* 427(6970):117–120.
2. Guo Q, et al. (2009) Reconstructing Earth's surface oxidation across the Archean–Proterozoic transition. *Geology* 37(5):399–402.
3. Lyons TW, Reinhard CT, Planavsky NJ (2014) The rise of oxygen in Earth's early ocean and atmosphere. *Nature* 506(7488):307–315.
4. Canfield DE (1998) A new model for Proterozoic ocean chemistry. *Nature* 396(6692): 450–453.
5. Konhauser KO, et al. (2011) Aerobic bacterial pyrite oxidation and acid rock drainage during the Great Oxidation Event. *Nature* 478(7369):369–373.
6. Planavsky NJ, Bekker A, Hofmann A, Owens JD, Lyons TW (2012) Sulfur record of rising and falling marine oxygen and sulfate levels during the Lomagundi event. *Proc Natl Acad Sci USA* 109(45):18300–18305.
7. Canfield DE, et al. (2013) Oxygen dynamics in the aftermath of the Great Oxidation of Earth's atmosphere. *Proc Natl Acad Sci USA* 110(42):16736–16741.
8. Rouxel OJ, Bekker A, Edwards KJ (2005) Iron isotope constraints on the Archean and Paleoproterozoic ocean redox state. *Science* 307(5712):1088–1091.
9. Poulton SW, Canfield DE (2011) Ferruginous conditions: A dominant feature of the ocean through Earth's history. *Elements* (*Quebec*) 7(2):107–112.

10. Planavsky NJ, et al. (2011) Widespread iron-rich conditions in the mid-Proterozoic ocean. *Nature* 477(7365):448–451.
11. Bekker A, et al. (2010) Iron formation: The sedimentary product of a complex interplay among mantle, tectonic, oceanic, and biospheric processes. *Econ Geol* 105(3): 467–508.
12. Planavsky N, et al. (2012) Iron isotope composition of some Archean and Proterozoic iron formations. *Geochim Cosmochim Acta* 80:158–169.
13. Johnson CM, Beard BL, Roden EE (2008) The iron isotope fingerprints of redox and biogeochemical cycling in modern and ancient Earth. *Annu Rev Earth Planet Sci* 36: 457–493.
14. Mathur R, et al. (2005) Cu isotopic fractionation in the supergene environment with and without bacteria. *Geochim Cosmochim Acta* 69(22):5233–5246.
15. Balistrieri LS, Borrok DM, Wanty RB, Ridley WI (2008) Fractionation of Cu and Zn isotopes during adsorption onto amorphous Fe(III) oxyhydroxide: Experimental mixing of acid rock drainage and ambient river water. *Geochim Cosmochim Acta* 72(2): 311–328.
16. Pokrovsky OS, Viers J, Emnova EE, Kompantseva EI, Freydier R (2008) Copper isotope fractionation during its interaction with soil and aquatic microorganisms and metal oxy(hydr)oxides: Possible structural control. *Geochim Cosmochim Acta* 72(7):1742–1757.
17. Ehrlich S, et al. (2004) Experimental study of the copper isotope fractionation between aqueous Cu(II) and covellite, CuS. *Chem Geol* 209(3-4):259–269.
18. Fernandez A, Borrok DM (2009) Fractionation of Cu, Fe, and Zn isotopes during the oxidative weathering of sulfide-rich rocks. *Chem Geol* 264(1-4):1–12.
19. Rodríguez NP, et al. (2015) Isotopic signature of Cu and Fe during bioleaching and electrochemical leaching of a chalcopyrite concentrate. *Int J Miner Process* 134:58–65.
20. Mathur R, Schlitt WJ (2010) Identification of the dominant Cu ore minerals providing soluble copper at Cañariaco Peru through Cu isotope analyses of batch leach experiments. *Hydrometallurgy* 101(1-2):15–19.
21. Fantle MS, DePaolo DJ (2004) Iron isotopic fractionation during continental weathering. *Earth Planet Sci Lett* 228(3-4):547–562.
22. Mathur R, et al. (2004) Cu isotopes and concentrations during weathering of black shale of the Marcellus Formation, Huntingdon County, Pennsylvania (USA). *Chem Geol* 304-305:175–184.
23. Kimball BE, et al. (2009) Copper isotope fractionation in acid mine drainage. *Geochim Cosmochim Acta* 73(5):1247–1263.
24. Rodríguez NP, et al. (2013) Copper and iron isotope fractionation in mine tailings at the Laver and Kristineberg mines, northern Sweden. *Appl Geochem* 32:204–215.
25. Wall AJ, Mathur R, Post JE, Heaney PJ (2011) Cu isotope fractionation during bornite dissolution: An in situ X-ray diffraction analysis. *Ore Geol Rev* 42(1):62–70.
26. Sherman DM (2013) Equilibrium isotopic fractionation of copper during oxidation/reduction, aqueous complexation and ore-forming processes: Predictions from hybrid density functional theory. *Geochim Cosmochim Acta* 118:85–97.
27. Liu S-A, et al. (2014) Copper and iron isotope fractionation during weathering and pedogenesis: Insights from saprolite profiles. *Geochim Cosmochim Acta* 146:59–75.
28. Takano S, Tanimizu M, Hirata T, Sohrin Y (2014) Isotopic constraints on biogeochemical cycling of copper in the ocean. *Nat Commun* 5:5663.
29. Kendall B, et al. (2010) Pervasive oxygenation along late Archaean ocean margins. *Nat Geosci* 3(9):647–652.
30. Ngombi-Pemba L, El Albani A, Meunier A, Grauby O, Gauthier-Lafaye F (2014) From detrital heritage to diagenetic transformations, the message of clay minerals contained within shales of the Palaeoproterozoic Francevillian basin (Gabon). *Precambrian Res* 255(Part 1):63–76.
31. Chi Fru E, et al. (2015) Arsenic stress after the Proterozoic glaciations. *Sci Rep* 5:17789.
32. Demory F, et al. (2005) Detrital input and early diagenesis in sediments from Lake Baikal revealed by rock magnetism. *Global Planet Change* 461(1-4):145–166.
33. Konhauser KO, et al. (2002) Could bacteria have formed the Precambrian banded iron formations. *Geology* 30(12):1079–1082.
34. Qu Y, Črne AE, Lepland A, van Zuilen MA (2012) Methanotrophy in a Paleoproterozoic oil field ecosystem, Zaonega Formation, Karelia, Russia. *Geobiology* 10(6):467–478.
35. Weber F, Gauthier-Lafaye F (2012) No proof from carbon isotopes in the Francevillian (Gabon) and Onega (Fennoscandian shield) basins of a global oxidation event at 1980–2090 Ma following the Great Oxidation Event (GOE). *C R Geosci* 345(1):28–35.
36. Kump LR, et al. (2011) Isotopic evidence for massive oxidation of organic matter following the great oxidation event. *Science* 334(6063):1694–1696.
37. Sperling EA, et al. (2015) Statistical analysis of iron geochemical data suggests limited late Proterozoic oxygenation. *Nature* 523(7561):451–454.
38. Guilbaud R, Butler IB, Ellam RM (2011) Abiotic pyrite formation produces a large Fe isotope fractionation. *Science* 332(6037):1548–1551.
39. Little SH, Vance D, Walker-Brown C, Landing WM (2014) The oceanic mass balance of copper and zinc isotopes, investigated by analysis of their inputs, and outputs to ferromanganese oxide sediments. *Geochim Cosmochim Acta* 125:673–693.
40. Little SH, Sherman DM, Vance D, Hein JR (2014) Molecular controls on Cu and Zn isotopic fractionation in Fe-Mn crusts. *Earth Planet Sci Lett* 396:213–222.
41. Manceau A, Nagy KL (2015) Comment on "Molecular controls on Cu and Zn isotopic fractionation in Fe-Mn crusts" by Little et al. *Earth Planet Sci Lett* 441:310–312.
42. Roy S (2006) Sedimentary manganese metallogenesis in response to the evolution of the Earth system. *Earth Sci Rev* 77(4):273–305.
43. Asael D, Mathews A, Bar-Mathews A, Halicz L (2007) Copper isotope fractionation in sedimentary copper mineralization (Timna Valley, Israel). *Chem Geol* 243(3-4):238–254.
44. Shlomovitch N, Bar-Matthews M, Matthews A (1999) Sedimentary and epigenetic copper mineral assemblages in the Cambrian Timna Formation, southern Israel. *Isr J Earth Sci* 48(140):195–208.
45. Mason TFD, et al. (2005) Zn and Cu isotopic variability in the Alexandrinka volcanic-hosted massive sulphide (VHMS) ore deposit, Urals, Russia. *Chem Geol* 221(3-4):170–187.
46. Rasmussen B, et al. (2012) Deposition of 1.88-billion-year-old iron formations as a consequence of rapid crustal growth. *Nature* 484(7395):498–501.
47. Farquhar J, Bao H, Thiemens M (2000) Atmospheric influence of Earth's earliest sulfur cycle. *Science* 289(5480):756–759.
48. Eriksson PG, Altermann W, Catuneanu O, van der Merwe R, Bumby AJ (2001) Major influences on the evolution of the 2.67–2.1 Ga Transvaal basin, Kaapvaal craton. Sediment Geol 141-142:205–231.
49. Maréchal CN, Telouk P, Albarede F (1999) Precise analysis of copper and zinc isotopic compositions by plasma-source mass spectrometry. *Chem Geol* 156(1-4):251–273.
50. Maréchal C, Albaréde F (2002) Ion-exchange fractionation of copper and zinc isotopes. *Geochim Cosmochim Acta* 66(9):1499–1509.
51. Malinovski D, et al. (2003) Performance of high resolution MC-ICP-MS for Fe isotope ratio measurements in sedimentary geological materials. *J Anal At Spectrom* 18(7): 687–695.
52. Rodushkin I, et al. (2015) Assessment of the natural variability of B, Cd, Cu, Fe, Pb, Sr, Tl and Zn concentrations and isotopic compositions in leaves, needles and mushrooms using single sample digestion and two-column matrix separation. *J Anal At Spectrom* 1(1):220–233.